Extreme Mechanics Letters 50 (2022) 101537

Contents lists available at ScienceDirect

Extreme Mechanics Letters

journal homepage: www.elsevier.com/locate/eml

Artificial stretchable armor for skin-interfaced wearable devices and soft robotics

Jungil Choi [a,1], Seungyong Han [b,1], Miguel Baliwag [c], Bong Hoon Kim [d,e], Hokyung Jang [f], Jin-Tae Kim [g], Insic Hong [b], Taewi Kim [b], Seong Min Kang [h], Kyu-Tae Lee [i], Daeshik Kang [b,*], John A. Rogers [g,j,k,l,**]

[a] School of Mechanical Engineering, Kookmin University, Seoul 02707, Republic of Korea
[b] Department of Mechanical Engineering, Ajou University, Suwon 16499, Republic of Korea
[c] Departments of Chemical Engineering, Northwestern University, Evanston, IL 60208, USA
[d] Department of Organic Materials and Fiber Engineering, Soongsil University, Seoul 06978, Republic of Korea
[e] Department of Smart Wearable Engineering, Soongsil University, Seoul 06978, Republic of Korea
[f] Department of Electrical and Computer Engineering, University of Wisconsin-Madison, Madison, WI 53706, USA
[g] Simpson Querrey Institute for Nano/Biotechnology, Northwestern University, Evanston, IL 60208, USA
[h] Department of Mechanical Engineering, Chungnam National University, Daejeon 34134, Republic of Korea
[i] Department of Physics, Inha University, Incheon 22212, Republic of Korea
[j] Center for Bio-Integrated Electronics, Northwestern University, Evanston, IL 60208, USA
[k] Departments of Materials Science and Engineering, Biomedical Engineering, Chemistry, Mechanical Engineering, Electrical Engineering and Computer Science, and Neurological Surgery, United States of America
[l] McCormick School of Engineering and Feinberg School of Medicine, Northwestern University, Evanston, IL 60208, USA

ARTICLE INFO

Article history:
Received 6 September 2021
Received in revised form 1 October 2021
Accepted 6 November 2021
Available online 25 November 2021

Keywords:
Stretchable armor
Overlapped structure
Wearable devices
Soft robotics

ABSTRACT

Animals such as the armadillo and pangolin have natural armor as a mechanical form of protection from predators. Among the several types of armor that exist in nature, structures composed of thin elastomeric substrates with overlapping hard scales can shield underlying soft tissues from physical impacts and localized stresses while maintaining a level of mechanical compliance necessary for natural motions. Here, we design and fabricate a class of artificial armor that derives inspiration from these natural systems. The optimization process involves systematic tests of several design candidates to assess their mechanical stability against different types of mechanical stresses. The resulting platforms provide highly effective protection layers for wearable electronic devices and soft robotic systems with little constraint on their functionality, as demonstrated with representative devices.

1. Introduction

Evolutionary forces have produced sophisticated forms of natural armor to protect certain classes of insects and animals from predators [1,2]. Particularly interesting examples are those that involve overlapping structures of mechanically tough materials joined by compliant underlying skins, as found in armadillos, pangolins and many species of fish. These hard/soft composite systems consist of rigid materials such as hardened mineral deposits, chitin, bone, or keratin with moduli in the range of GPa [2] joined and supported by sheets of soft collagen fibers with moduli in the range of MPa. In armadillos (*Dasypus novemcinctus*) the hard components take the form of scales, known as osteoderms, that have hexagonal shapes in the pectoral and pelvic regions and triangular shapes in the banded shield region. The large area of armor at the pectoral and pelvic regions consists of a single rigid structure without overlap, which leads to strong protection but with limitations on movement of the body [3]. By contrast, the armor of a pirarucu (*Arapaima gigas*), one of the largest types of freshwater fish, involves scales across the entire surface of the animal, where 60%–70% of each scale overlaps with adjacent scales. As joined by a soft internal collagen layer, this configuration provides considerable flexibility, with ability to adapt naturally to motions of the body. The pangolin (Fig. 1a) adopts a similar strategy in its armor, with overlapping keratinous scales [4]. Here, the scales and skin make up about 25 wt% of the body mass and the scales cover most of the animal [5]. The scales originate from

* Corresponding author.
** Corresponding author at: Simpson Querrey Institute for Nano/Biotechnology, Northwestern University, Evanston, IL 60208, USA.
E-mail addresses: dskang@ajou.ac.kr (D. Kang), jrogers@northwestern.edu (J.A. Rogers).
[1] These authors contributed equally to this work.

https://doi.org/10.1016/j.eml.2021.101537
2352-4316/

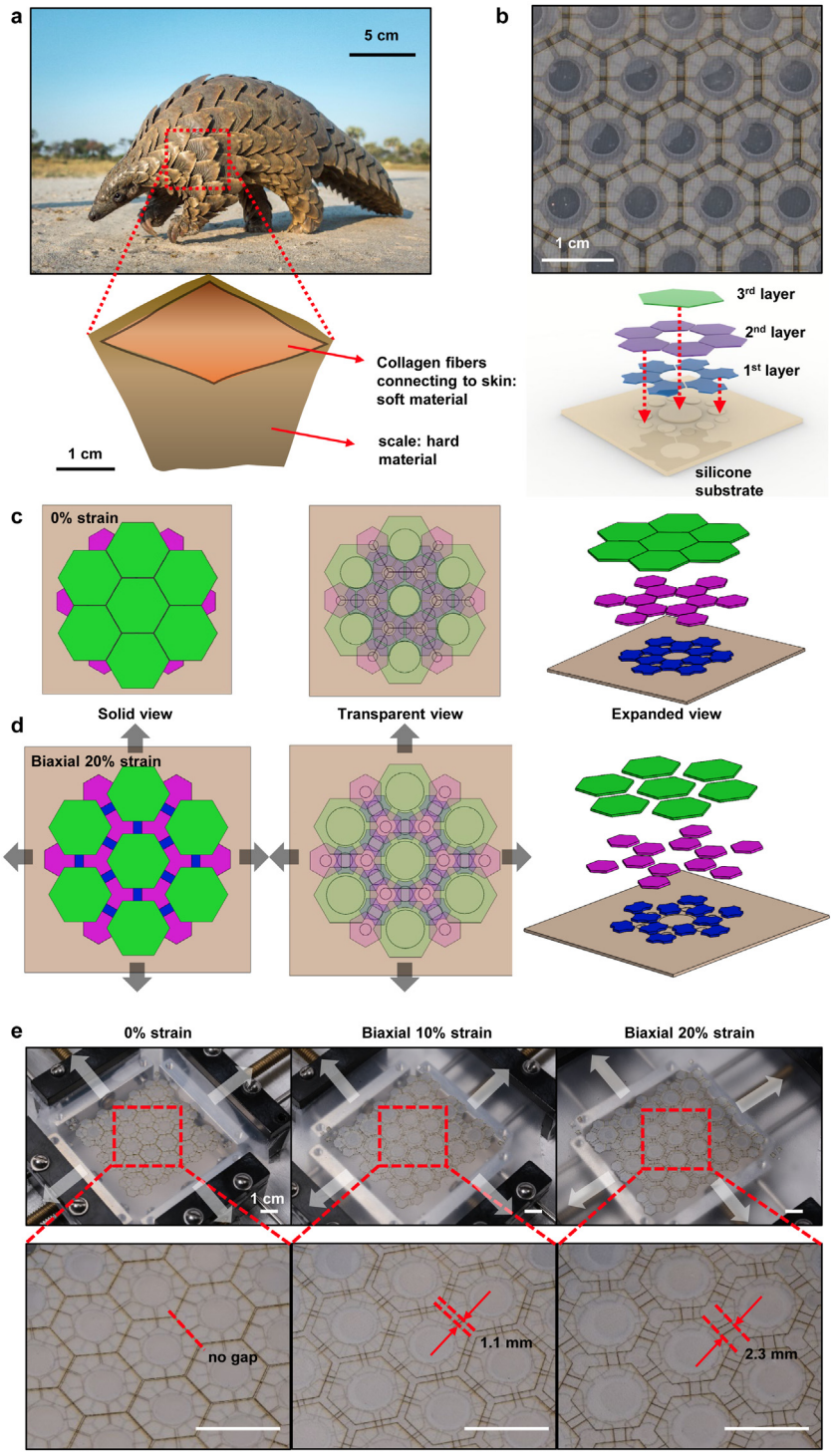

Fig. 1. Illustrations of natural and artificial stretchable armor. (a) Photograph of a pangolin and schematic illustration of the structure of the armor, composed of a soft substrate and hard scales in overlapping configurations. (b) Photograph of a representative artificial stretchable armor (ASA) during biaxial stretching (top) and the exploded view illustration of the design, highlighting the different layers of scales in different colors. (d) Schematic illustration of the ASA at (c) 0% strain and (d) biaxial strain of 20% in top view (solid color, left; semitransparent color, right) and in exploded view (right). (e) Photograph of a sample of ASA (top) and its magnified image (bottom) at 0% strain (left), biaxial strain of 10% (middle) and biaxial strain of 20% (right). Red dotted lines show the edges of scales and the related lengths show the distance between the scales. (a) Copyright 2021, Dana Allen PhotoSafari-Africa.net, adapted with permission.. (For interpretation of the references to color in this figure legend, the reader is referred to the web version of this article.)

the thick skin and continue to grow throughout the life of the animal, like the hair and the claws. The overlap of the internal and external surfaces are 30%–70% and 20%–40%, respectively [4].

Several examples of synthetic armor structures with this design strategy appear in the literature [6–10]. Examples of hard materials used in such systems include alumina [8], cellulose acetate butyrate [9], glass [3] and silicon [11] supported by soft substrates of polyurethane [8], polypropylene mesh [12], poly(dimethylsiloxane) [11] and silicone [3]. Detailed studies in these various cases define quantitative physical parameters associated with the key characteristics, but without the context of specific applications. The focus of the work presented here

is in the construction of related classes of armor, designed for use in two promising emerging technologies, epidermal electronics/microfluidics and soft robotics. The latter devices involve thin flexible, and sometimes stretchable, substrates that integrate sensors, actuators and/or microfluidic networks, often with supporting circuits, radios and power supplies, in ways that offer skin-compatible physical forms [13–16]. Conformal contact with the skin enables continuous measurements of biophysical and biochemical parameters associated with physiological status, often with clinical-grade levels of accuracy. Protection of these soft devices from mechanical impact can be important in many practical scenarios. Similar considerations apply to soft robotic systems, where elastomeric materials and inflatable bladders controlled by pneumatic or hydraulic pressure serve as the basis for locomotion, manipulation and other core functions [17–19].

The results presented here feature designs in protective, artificial stretchable armor (ASA) for these two classes of technologies. Systematic mechanical tests of several overlapped designs inspired by pangolin skins define key considerations and reveal optimized layouts. A complementary triple layer configuration emerges as a scheme that provides outstanding levels of protection with high levels of stretchability. Examples of applications with representative epidermal electronic and microfluidic devices demonstrate possibilities in skin-integrated systems. Implementation in multigate soft robots illustrates the applicability of related ASAs in this area of technology.

2. Results and discussion

2.1. Multi-layered structural artificial stretchable armor

The basic scheme of the ASAs explored here involves hard material structures partially bonded to soft material substrates in an overlapping configuration (Fig. 1b) [11]. Composites of fiber glass and epoxy (Garolite) serve as the scales of the ASA due to their large Young's modulus (∼20 GPa), high physical toughness [20] and relatively low density (∼1.8 g/cm^3) [21]. The specific systems reported here include scales with thicknesses of 127 μm in three layers bonded to posts formed on the surfaces of a 500 μm thick silicone substrate (Ecoflex) (Fig. S1). The first layer of scales has irregular hexagonal shapes with widths of 3 mm. The second and third layers adopt hexagonal shapes with diagonal lengths of 5.8 mm and 10 mm, respectively (Fig. S2). Hexagonal shapes of scales in the top layer guarantee coverage across all the region of substrate. The total thickness of the resulting ASA is 1 mm, for thin and flexible construction, with the ability to stretch. In one design that shows excellent characteristics, three layers of scales cover the entire area of the soft substrate in its strained and unstrained states. Only the top layer is visible in the condition without applied strain, such that the other layers remain hidden below the third layer (Fig. 1c). At 20% biaxial strain, the second layer covers the regions that open between the scales of the first layer, and the first layer covers the region associated with the second layer, thereby providing protection across the entire area of the soft substrate. (Fig. 1d) The maximum strain for triple layer enabling the full coverage is 40% in ideal case. Fig. 1e shows the behavior of the third layer of scales at 0%, 10%, and 20% biaxial strain. For the latter two cases, the gaps between the scales of the top layer are 1.1 and 2.3 mm, respectively. At 20% biaxial strain, the 2.3 mm gaps of the top layer are fully covered by the scales of the second and the first layers because the size of the scales are 5.8 mm in diagonal length and 3.0 mm in width, respectively. (Fig. 1e) This type of ASA can smoothly bend over a curved surface with various levels of curvature such that the gaps in the top layer remain covered by the first and second layer (Fig. S3).

2.2. Mechanical stability of artificial stretchable armor

The scales can protect the underlying materials from damage due to mechanical forces associated with pressure applied using both sharp and blunt needles, and with sudden physical impacts. Pressure delivered in these ways can lead to failures associated with puncture of the scales or with strong tilting motions of them to expose the underlying materials (Fig. 2a). Stretchable armor that involves scales in single layer, double layer, triple layer, maximum (max) triple layer, and maximum (max) triple layer with double thickness designs exhibit different levels of protection against these failure modes (Fig. 2b and S4). Quantitative measurements use controlled pressures (MTS testing machine) delivered with sharp and blunt needles at various locations across a given scale: corner (Fig. 2c and S3), middle (between center and edge; Fig. 2d and S3), and center (Fig. 2e and S3). In the case of corners, where gaps between scales in third-layer exist, the minimum forces that lead to puncture, which we refer to as critical forces, for the sharp and blunt needles range from 0.33 N to 7.1 N and from 1.3 to 6.1 N, respectively (Fig. 2c). Pressing the needle at the midpoint between the center and the edge, yields larger critical forces than those on the edge due to the overlapping structure of the scales and their structural stability (Fig. 2d). When the needles press at the center of the ASA, the critical forces for sharp and blunt needles are 5.3 N for the single layer and 21 N for double thickness layer designs, both much higher than those for the other cases (Fig. 2e). However, the critical puncture force for the max triple layer is similar with the previous case because the numbers of overlapped layers at the contact point for both are identical. For a blunt needle, the critical force significantly increases as the contact point moves to the center, due to an increase in structural stability and absence of tilting motions. The critical forces of the single and double layer are larger than those of triple layers. In these cases, tilting dominates the case of failure of the ASA under pressure, such that increasing the number of layers in the ASA, to triple layers, increases the chance of tilting the ASA due to the larger thickness of the structure. Overall, the ASA with max triple layer with double thickness shows the best performance in protection. However, as the flexibility and overall thickness are important criteria for applications in wearable devices and soft robots, the ASA with max triple layer serves the main design for the following experiments.

Tests associated with blunt needle impacts address other aspects of the protective function. Here, the focus is on ASAs with the max triple layer design, due to its good performance under such scenarios (Fig. 2f). Evaluation involves dropping a weight with a blunt protrusion on its surface against an ASA placed on top of a plate of glass. Without ASA protection, the glass fractures at heights above ∼7 cm, corresponding to kinetic energies larger than 0.21 J. With the ASA, fractures initiate at the kinetic energies of 0.73, 1.0, and 1.9 J for impacts at the center, edge and corner of the scale structure, respectively (Fig. 2g and S5). In the case of impacting at the center where only one layer of scale exists, the soft substrate absorbs a large fraction of the physical impact. However, when the weight drops at the corner of the scale where the scales overlaps, the crack generating energy increased by 2.5 times compared to that at the center. The centers of the scales involve only one layer of epoxy glass, whereas three layers exist at the corners. These results follow from the overlapping design of the triple layer system with the soft substrate.

For applications in epidermal electronics and soft robotics considered here, the mechanical properties, such as modulus and stiffness, of the ASA are critical to maintain the overall stretchability of the integrated system. Fig. 2h shows strain–stress curves associated with the soft substrate of an ASA with the max triple layer design formed using a similar substrate. The modulus of

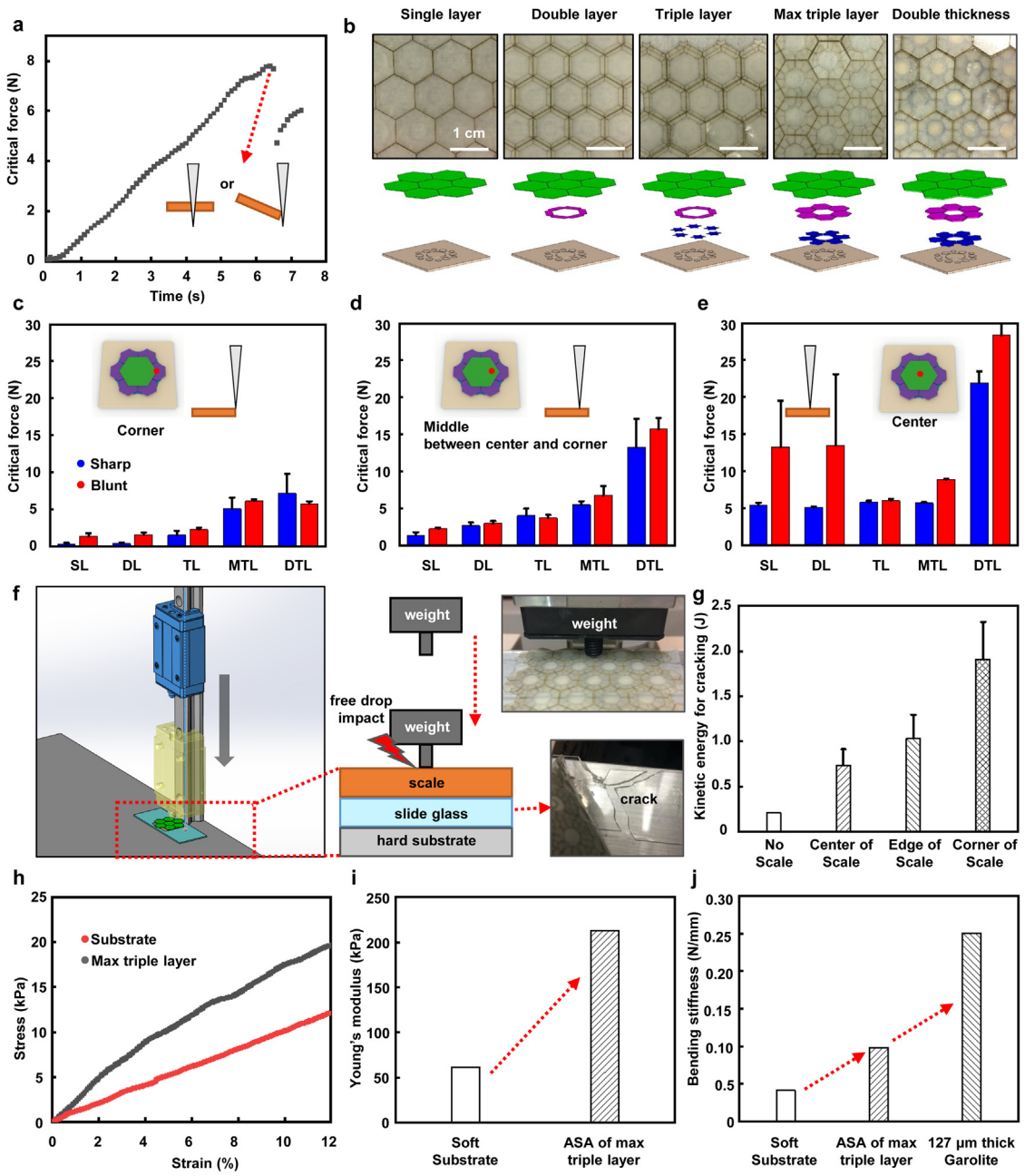

Fig. 2. Mechanical characterization of ASA samples with various design layouts. (a) Graph of applied force as a function of time and schematic illustration of the puncture and tilt failure modes. (b) Photographs (top) and schematic illustrations (bottom) of design layouts of ASA samples evaluated here, denoted single, double, and triple layer, max triple layer, double thickness layer. Histogram plots of critical forces for inducing either puncture or tilt mode failures for pressure applied using sharp (blue) and blunt (red) needles at the (c) edge, (d) middle between the center and edge, and (e) center to different ASA samples. SL: Single layer, DL: Double layer, TL: Triple layer, MTL: Max triple layer, and DTL: Double thickness layer (f) Schematic illustrations and photographs of impact testing that involves dropping a weight with a round tip onto a piece of glass covered by a sample of ASA. (g) Histogram plot of the kinetic energy associated with cracking of the glass for different cases. (h) Strain–stress relationship for an elastomeric substrate with and without an ASA with a max triple layer design. (i) Histogram plot of the Young's modulus of an elastomeric substrate with and without an ASA with max triple layer design. (j) Histogram plot of bending stiffness of an elastomeric substrate with and without an ASA with a max triple layer design, and a sheet of Garolite with thickness of 127 μm.. (For interpretation of the references to color in this figure legend, the reader is referred to the web version of this article.)

the ASA is higher than that of the substrate by ∼3.5 times due to mechanical loading that follows from the presence of non-stretchable regions at the locations where the substrate bonds to the scales (Fig. 2i). Similarly, the bending stiffness of the ASA is higher than the substrate by approximately a factor of two (0.04 N/mm vs. 0.09 N/mm) (Fig. 2j). The stiffness of the ASA is, of course, much smaller than that of the material of the scales. Finite element analysis (FEA) of displacements under identical tensile stresses and three-point bending forces applied to the soft substrate and the ASA show a decrease in the displacement of ASA compared to the soft substrate, implying an increase in modulus and bending stiffness, as expected (Fig. S6).

2.3. Applications of ASA to epidermal electronics

Epidermal electronic systems typically include some combination of hard and soft electronic components integrated in a strategic fashion on a thin, flexible, stretchable substrate to yield

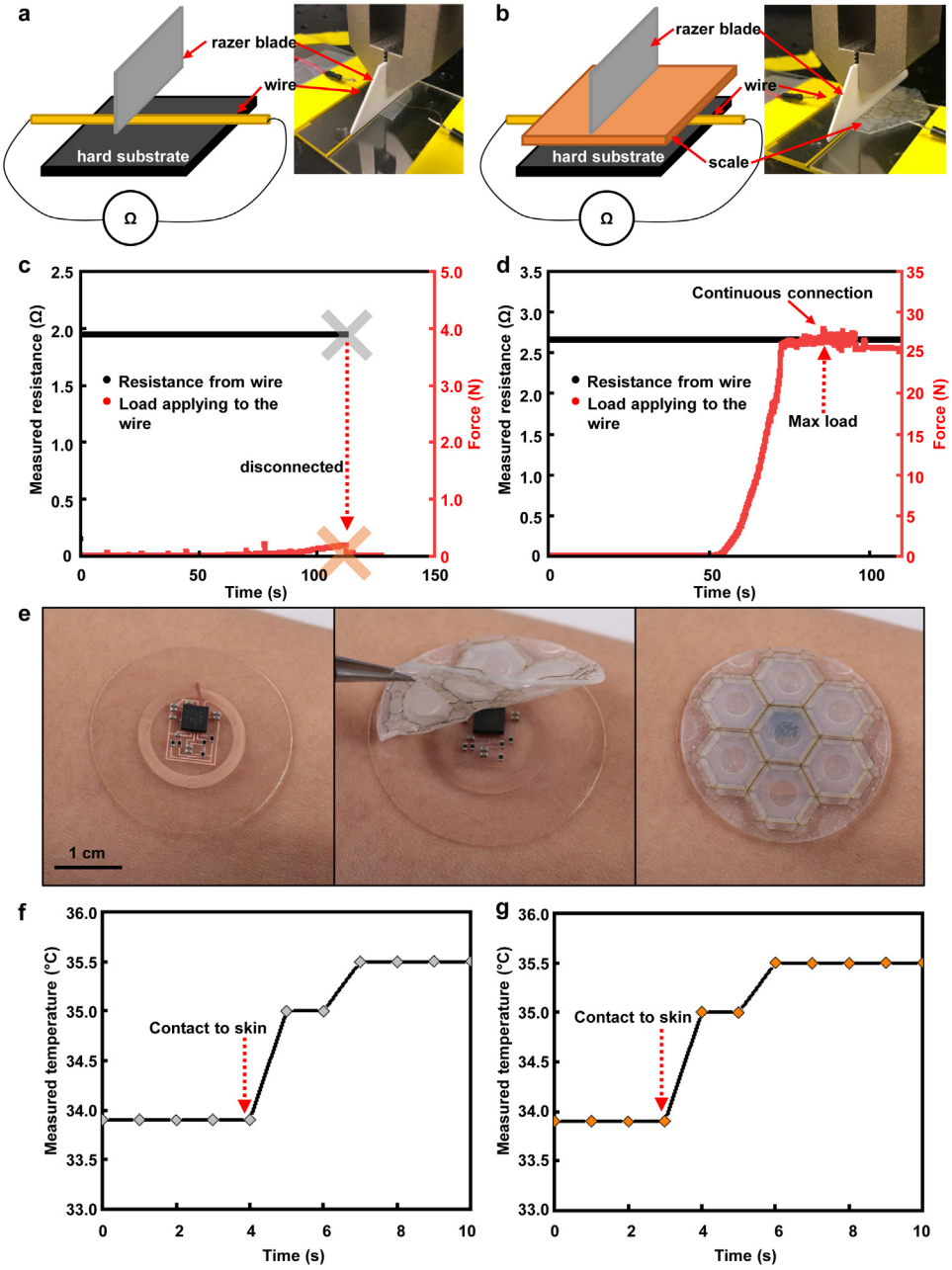

Fig. 3. Applications of ASA to epidermal electronic devices. Schematic illustrations and photographs of the procedure for testing the ability of an ASA to protect a conducting wire from cutting force delivered with a razor blade, by comparing cases (a) without and (b) with the ASA. Graph of the resistance the wire as a function of applied force (c) without and (d) with ASA. Photograph of a representative wireless epidermal electronic device for measuring skin temperature before (left), during (middle) and after (right) lamination of a ASA on top. Graphs of temperature measured using the device (f) without and (g) with the ASA.

a skin-like set of physical properties [13]. As such, these types of devices can be damaged by mechanical forces. The ASAs introduced here can provide a protective overlayer, without sacrificing stretchability or interfering with the function of the device or its interface to the skin. A simple validation involves placing an ASA on top of a thin coil designed to support near field communication (NFC) protocols, to compare its resistance to cutting with a razor blade to the case without the ASA (Fig. 3a and b). The bare coil severes at a force of ∼0.18 N (Fig. 3c). Adding the ASA increases this value to 25 N (Fig. 3d). Fig. 3e shows an example of an ASA applied to an epidermal electronic device designed for wireless NFC measurements of skin temperature, with a coil thickness of 18 μm and a width of 150 μm on a PDMS substrate (∼1 mm thick). The ASA (max triple layer design) does not interfere with wireless communication because the constituent materials (epoxy-glass and silicone) have low permeability and conductivity. (Fig. 3f) The weight of the ASA in Fig. 3e is only 0.5 g, suitable for wearable applications. ASA samples formed with transparent materials such as polyethylene terephthalate provide both protection and optical access, of use with colorimetric microfluidic devices for sweat analysis (Fig. S7).

2.4. Applications of ASA to soft robotics

Soft robotic systems often use pneumatic pressure as a primary means for actuation, through structures that combine stretchable material features with air-channels and relatively rigid base layers [22]. Here, mechanical protection is important to avoid punctures and associated points of leakage. The protective

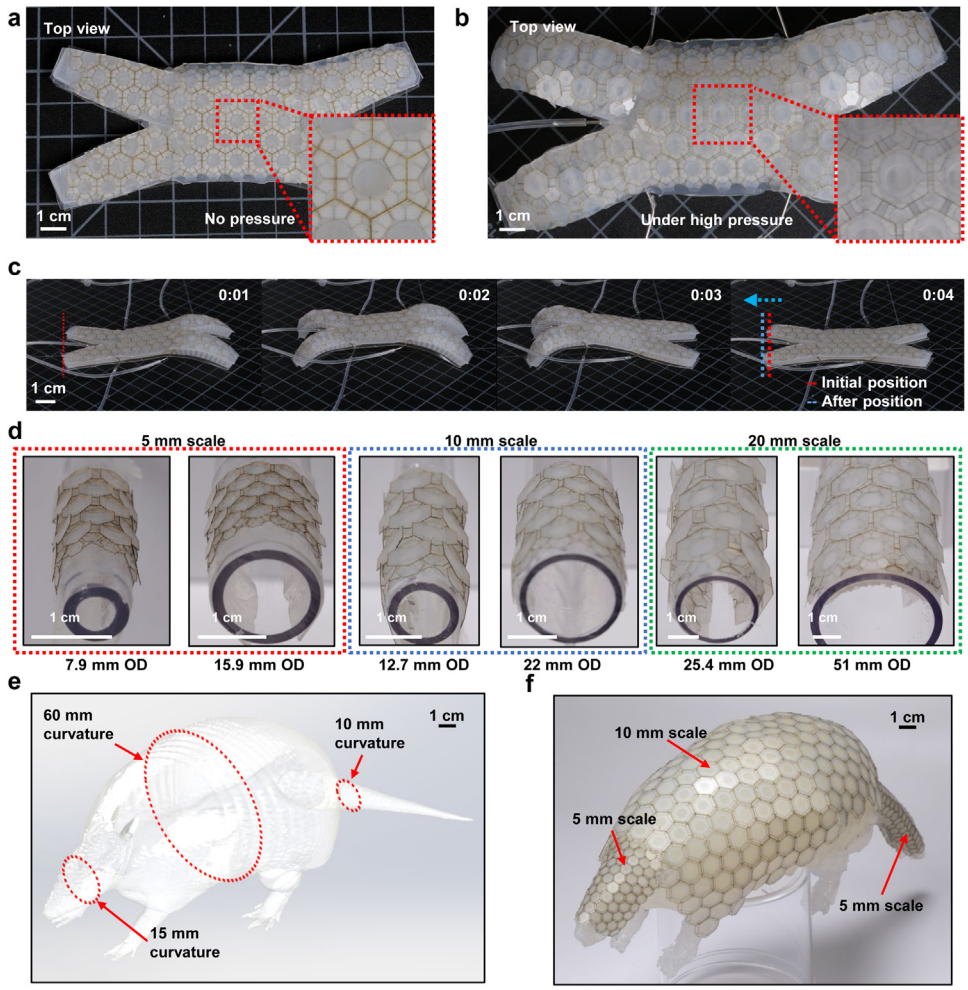

Fig. 4. Applications of ASA to soft robotic systems. Photographs of a multigate soft robot with an ASA at (a) no pressure (b) under high pressure. The inset shows magnified images of the ASA. (c) Time-sequence of photographs of the robot with control of pressure to generate forward movement. (d) Photographs of an ASA with different scale sizes of 5 (left), 10 (middle), and 15 mm (right) on cylinders with diameters from 7.9 mm to 51 mm. (e) Schematic illustration of a structure in the shape of an Armadillo, with radius of curvature values for various parts of the body. (f) Photograph of an Armadillo model covered with pieces of ASA designed with scales at sizes tailored to the various radii of curvature.

structures must, however, allow the robot to move without constraint, as achieved with ASA structures summarized in Fig. 4a–c. Here, a triple-layered ASA bonds to the top surface of a multigate soft robot. Without pressure, the ASA is in a closed state (Fig. 4a). Upon application of air pressure, the top layer of the soft robot expands, and the ASA simultaneously stretches without exposing the underlying soft substrate (Fig. 4b) Coordinated application of air pressure allows the soft robot to move forward with a gait that is unaffected by the ASA (Fig. 4c) The layers of ASA can be provided with patterns of coloration as a camouflage, even in the stretched condition (Fig. S7). Robots with complex curvatures and different dimensions benefit from ASAs with different scale geometries. Wrapping ASA platforms built with scales with dimensions of 5, 10, and 15 mm around cylinders with outer diameters from 7.9 to 15.9 mm, 12.7 to 22 mm, and 25.4 to 51.0 mm, respectively (Fig. 4d, S3) illustrates the effects. A 3D model of an armadillo highlights various curvatures at different parts of the anatomy, from 10 mm at the tail, to 15 mm at the head to 60 mm at the torso. ASA platforms with scales of 5 mm and 10 mm bonded at different relevant locations provides full coverage across the relevant surfaces.

3. Conclusions

In summary, this paper introduces artificial stretchable armors that mimic the designs of natural armor in animals. The overlapped structures of the scales and integration to the soft substrate yields stretchable armors that provide protection without sacrificing the soft mechanics of the system. Various mechanical tests validate the protection capabilities of the ASA. Applications in epidermal electronics and soft robotics establish the applicability of ASAs to the devices of these types, without adverse effects on their performance. The results suggest these types of ASAs form attractive options for the protection of skin-interfaced devices and pneumatically controlled robots. Combined use of these designs with electronics and functional materials provides a wide range of engineering options in the fabrication of physical protection for various environmental conditions and application scenarios.

4. Materials and methods

4.1. Fabrication of silicon molds for the soft substrates

Posts with three different heights molded onto the surface of a soft substrate served as bonding locations for the three different

layers of scales. The fabrication began with the formation of a silicon mold by spin coating a layer of photoresist (KMPR 1010, Microchem, MA, USA) at 3000 rpm for 30 s on a silicon wafer (1.5 mm thickness), performing photolithography and then deep reactive ion etching (STS Pegasus ICP-DRIE; SPTS Technologies, Newport, UK) to recessed features to a depth of 120 μm on the surface of the wafer. A similar process defined features with depths of 240 and 360 μm on the same wafer. Spin-coating poly(methylmethacrylate) (PMMA; Microchem, MA, USA) at 3000 rpm followed by curing at 180 °C generated a layer to facilitate demolding of a soft substrate formed using a platinum-catalyzed silicone (Ecoflex 0035; Smooth-On, Inc., PA, USA) spin-cast at 200 rpm and cured at room temperature for 5 min.

4.2. Fabrication of stretchable armor

Pouring PDMS (Sylgard 184; Dow corning, MI, USA; mixing ratio of base to curing agent: 10:1) on a PMMA-coated silicon wafer and spin-casting at 200 rpm generated a temporary substrate as a support for a sheet of fiberglass-epoxy (127 μm thick; Garolite, G-10/FR4, IL, USA) placed on top. An automated laser cutting system (CO_2 laser, Universal Laser Systems, AZ, USA) defined the outline of the hard scales, cleaned by wiping with isopropyl alcohol. After removing the unnecessary parts of the scales, corona treating (1 min) these scales and the soft substrate layer of platinum-catalyzed silicone enabled strong bonding between them upon contact with mild pressure for 1 min.

4.3. Fabrication of soft robots with stretchable armor

A stereolithography apparatus served as a 3D printing tool (Form2; Formlabs, MA, USA) to generate the molds for the soft robots. Pouring platinum-catalyzed silicone (Ecoflex 0030; Smooth-On, Inc., PA, USA) and thermal curing in the mold generated the main body of the robot with an air channel. Spin coating 10:1 PDMS at 150 rpm on a 5-inch silicon wafer generated the bottom layer of the robot. Spin coating of Ecoflex 0035 at 1000 rpm on the PDMS formed a layer to serve as an adhesive bond. The body of the robot was attached to the uncured Ecoflex on PDMS and cured at 70 °C for 1 h. Ecoflex 0035 was coated on the top of the soft robot, and the stretchable armor was then bonded on the top. A needle connected with tubing to an N_2 gas cylinder was placed on the side of the robot to generate movement.

4.4. Mechanical testing of the stretchable armor

A tensile tester (20G: MTS Sintech) yielded stress/strain responses and three-point bending stiffness results. A custom stage enabled the stretching tests. A force gauge (Mark-10, NY, USA) determined the forces associated with the pressing tests. A sharp needle with a diameter of 0.91 mm and a blunt tip with a radius of 1 mm served to pucture the ASA. For the cutting tests, copper metal wire with a thickness of 18 μm and width of 150 μm was used. A 300 g ball bearing carriage with circular blunt protrusion fell along a guide rail for the free drop test. The contact area with the scale was 7 mm^2 at the circular tip.

4.5. Fabrication of the NFC-based epidermal electronic device

For the epidermal NFC device, a copper foil (18/5 μm thick, Oak Mitsui MicroThin Series) served as the main material for the coil and electrical interconnects. After conformal lamination of copper foil onto a PDMS (Sylgard 184, Dow-Corning, monomer: curing agent = 5: 1 weight ratio) coated soda-lime glass microscope slide, the coil and interconnects were patterned by a conventional photolithography process (photoresist AZ P4620, AZ Electronic Materials Corporation) and wet etching (CE-100 copper etchant). The photoresist was removed with acetone/DI water, and electrical circuit components (ams AG; NFC die SL13A) were assembled onto the circuit patterns. Finally, the device was detached from the glass slide using a water-soluble tape (Smart-solve Inc.) and transfer-printed on a PDMS substrate (thickness ∼1 mm). For testing the interference of the ASA with wireless communication by NFC device, the NFC sensor (RF430FRL152H, Texas Instruments, TX, USA) was fabricated on a flexible printed circuit board with a thickness of 50 μm. A smartphone with NFC interface (Samsung Galaxy S8, Samsung, South Korea) read the temperature data from the sensor.

Declaration of competing interest

The authors declare that they have no known competing financial interests or personal relationships that could have appeared to influence the work reported in this paper.

Acknowledgments

J.C. and S.H. contributed equally to this work. This work utilized Northwestern University Micro/Nano Fabrication Facility (NUFAB), which is supported in part by Soft and Hybrid Nanotechnology Experimental (SHyNE) Resource, USA (NSF ECCS-154 2205), the Materials Research Science and Engineering Center, USA (DMR-1720139), the State of Illinois, and Northwestern University, USA. The authors thank the Center for Bio-Integrated Electronics for support of this work. This work was supported by the National Research Foundation of Korea (NRF) grant funded by the Korea government (MSIT) (NRF-2019R1A2C1084419, 2019R1C1C1 007629,2019R1A2C1090056); and the Ministry of Trade, Industry & Energy (MOTIE, Korea) under Industrial Technology Innovation Program. (No. 20000512); and the Environmental Health Action Program (Development of receptor-based environment-induced diseases prevention and management system using real-time collected environment and health information) under Project 2018001350005; and the Korea Evaluation Institute of Industrial Technology (KEIT) (1415175191) funded by the Ministry of Trade, Industry & Energy, Republic of Korea; and the Ajou University research fund, South Korea.

References

[1] D.J. Zhu, et al., Structure and mechanical performance of a modern fish scale, Adv. Energy Mater. 14 (4) (2012) B185–B194.
[2] W. Yang, et al., Flexible dermal armor in nature, Jom 64 (4) (2012) 475–485.
[3] R.K. Chintapalli, et al., Fabrication, testing and modeling of a new flexible armor inspired from natural fish scales and osteoderms, Bioinspiration Biomim. 9 (3) (2014).
[4] B. Wang, et al., Pangolin armor: Overlapping, structure, and mechanical properties of the keratinous scales, Acta Biomater. 41 (2016) 60–74.
[5] A. Bartholomai, East-African mammals - an Atlas of evolution in Africa, Vol 3, Pt C, Pt D - Kingdon, J. Search 14 (7–8) (1983) 224.
[6] M.M. Porter, et al., 3D-printing and mechanics of bio-inspired articulated and multi-material structures, J. Mech. Behav. Biomed. Mater. 73 (2017) 114–126.
[7] R. Martini, F. Barthelat, Stability of hard plates on soft substrates and application to the design of bioinspired segmented armor, J. Mech. Phys. Solids 92 (2016) 195–209.
[8] R. Martini, F. Barthelat, Stretch-and-release fabrication, testing and optimization of a flexible ceramic armor inspired from fish scales, Bioinspiration Biomim. 11 (6) (2016) 066001.
[9] N. Funk, et al., Bioinspired fabrication and characterization of a synthetic fish skin for the protection of soft materials, ACS Appl. Mater. Interfaces 7 (10) (2015) 5972–5983.
[10] R. Martini, Y. Balit, F. Barthelat, A comparative study of bio-inspired protective scales using 3D printing and mechanical testing, Acta Biomater. 55 (2017) 360–372.

[11] S. Kim, et al., Imbricate scales as a design construct for microsystem technologies, Small 8 (6) (2012) 901–906.
[12] N. Funk, et al., Bioinspired fabrication and characterization of a synthetic fish skin for the protection of soft materials, Acs Appl. Mater. Interfaces 7 (10) (2015) 5972–5983.
[13] T.R. Ray, et al., Bio-integrated wearable systems: A comprehensive review, Chem. Rev. 119 (8) (2019) 5461–5533.
[14] D.H. Kim, et al., Epidermal electronics, Science 333 (6044) (2011) 838–843.
[15] J. Choi, et al., Skin-interfaced systems for sweat collection and analytics, Sci. Adv. 4 (2) (2018).
[16] R. Ghaffari, et al., Soft wearable systems for colorimetric and electrochemical analysis of biofluids, Adv. Funct. Mater. 30 (37) (2020).
[17] M. Calisti, G. Picardi, C. Laschi, Fundamentals of soft robot locomotion, J. R. Soc. Interface 14 (130) (2017).
[18] P. Polygerinos, et al., Soft robotics: Review of fluid-driven intrinsically soft devices; manufacturing, sensing, control, and applications in human-robot interaction, Adv. Energy Mater. 19 (12) (2017).
[19] C. Lee, et al., Soft robot review, Int. J. Control Autom. Syst. 15 (1) (2017) 3–15.
[20] B. Shen, G.H. Paulino, Direct extraction of cohesive fracture properties from digital image correlation: A hybrid inverse technique, Exp. Mech. 51 (2) (2011) 143–163.
[21] G.S. Chandekar, B.S. Thatte, A.D. Kelkar, On the behavior of fiberglass epoxy composites under low velocity impact loading, Adv. Mech. Eng. (2010).
[22] R.F. Shepherd, et al., Multigait soft robot, Proc. Natl. Acad. Sci. USA 108 (51) (2011) 20400–20403.